Applied Surface Science 648 (2024) 159057

Contents lists available at ScienceDirect

Applied Surface Science

journal homepage: www.elsevier.com/locate/apsusc

Full Length Article

Controlling the magnetic properties of layered Cr_2Te_3 thin films via ex-situ annealing

In Hak Lee [a,*], Yeong Gwang Khim [b,c], Jaeun Eom [a,d], Jung Yun Kee [a,e], Byoung Ki Choi [f], Hyuk Jin Kim [b,c], Ryung Kim [g], Min Young Jung [g], Kyeong Jun Lee [g], Younghak Kim [h], Woo-Suk Noh [i], Byeong-hyeon Lee [j], Hoyoung Suh [j], Hye Jung Chang [j], Sung Ok Won [j], Chaun Jang [a], Hyejin Ryu [a], Dong Ryeol Lee [e], Seo Hyoung Chang [g], Hyun Hwi Lee [h], Young Jun Chang [b,c,k,*], Jun Woo Choi [a,*]

[a] Center for Spintronics, Korea Institute of Science and Technology (KIST), Seoul 02792, South Korea
[b] Department of Physics, University of Seoul, Seoul 02504, South Korea
[c] Department of Smart Cities, University of Seoul, Seoul 02504, South Korea
[d] Department of Physics and Astronomy, Seoul National University, Seoul 08826, South Korea
[e] Department of Physics, Soongsil University, Seoul 06978, South Korea
[f] Advanced Light Source, Lawrence Berkeley National Laboratory, Berkeley, CA 94720, USA
[g] Department of Physics, Chung-Ang University, Seoul 06974, South Korea
[h] Pohang Accelerator Laboratory, POSTECH, Pohang 37673, South Korea
[i] MPPC-CPM, Max Planck POSTECH/Korea Research Initiative, Pohang 37673, South Korea
[j] Advanced Analysis Center, Korea Institute of Science and Technology (KIST), Seoul 02792, South Korea
[k] Department of Intelligent Semiconductor Engineering, University of Seoul, Seoul 02504, South Korea

ARTICLE INFO

Keywords:
van der Waals magnetic materials
Cr_2Te_3 thin films
Ex-situ annealing
Curie temperature
Lattice expansion

ABSTRACT

We present a post-growth ex-situ annealing method to control the Curie temperature and magnetic anisotropy of Cr_2Te_3 van der Waals ferromagnetic thin films. The as-grown Cr_2Te_3 films exhibit a Curie temperature ~ 170 K with an out-of-plane magnetic easy axis. Upon high temperature (300 – 400 °C) ex-situ annealing, the magnetic phase of the film changes: the Curie temperature is significantly increased to ~ 300 K and the magnetic easy axis is reoriented to the in-plane direction. Electronic, chemical, and structural analyses suggest that the c-axis lattice constant expansion, accompanying the annealing process, is the origin of the ex-situ-annealing-induced modulation of the Cr_2Te_3 film magnetic properties. These results demonstrate that a practical ex-situ annealing process can be effectively used to control the magnetic properties of van der Waals ferromagnetic thin films. Furthermore, the room temperature ferromagnetic ordering emerging upon annealing, along with its robustness against post-growth thermal processes, suggests that the Cr_2Te_3 thin film is a promising magnetic material candidate for potential application in van-der-Waals-material-based spintronic devices.

1. Introduction

Magnetic and spin-transport properties of van der Waals (vdW) magnetic materials have been extensively studied in the last few years [1–13]. These layered magnetic materials, composed of two-dimensional (2D) planes stacked by vdW interactions, provide an ideal platform for fundamental investigation of low-dimensional magnetism, along with related spin, charge, and topological phenomena [14–23]. Furthermore, spintronic devices consisting of vdW magnets offer unique advantages over conventional magnetic material systems. Heterostructure devices, composed of various families of vdW materials, possess clean and well-defined interfaces, making it possible to systematically study emergent interfacial electronic- and spin-transport phenomena. Yet, there remains several major obstacles that need to be overcome for integration of 2D/vdW-magnetic-material-based spintronic devices into commercial electronics [24–26]. In particular, large scale thin film growth of vdW magnetic materials which exhibit room temperature ferromagnetism is required. Additionally, it would be

* Corresponding authors at: Department of Physics, University of Seoul, Seoul 02504, South Korea (Y.J. Chang).
E-mail addresses: ihl88@kist.re.kr (I.H. Lee), yjchang@uos.ac.kr (Y.J. Chang), junwoo@kist.re.kr (J.W. Choi).

https://doi.org/10.1016/j.apsusc.2023.159057
Received 13 September 2023; Received in revised form 14 November 2023; Accepted 29 November 2023
Available online 3 December 2023

advantageous if the material characteristics are sustained under high temperature and atmospheric conditions, such that it can endure back end of line fabrication processes in the semiconductor industry [27,28].

In this regard, $Cr_{1+x}Te_2$ compounds are adequate material systems to ultimately achieve this objective, as epitaxially grown ultrathin films of this material exhibit room temperature ferromagnetism along with highly tunable magnetic characteristics [6,9,29–33]. Each layer of $CrTe_2$ ($x = 0$) consists of a middle Cr plane sandwiched between outer Te planes, with vdW stacking of the layers. In $Cr_{1+x}Te_2$, Cr atoms are intercalated in the vdW gap of $CrTe_2$ with increasing x, i.e., increasing Cr content, resulting in modulation of its magnetic properties [19,34–37]. $Cr_{1+x}Te_2$ show variation in magnetic anisotropy and Curie temperature (T_C) depending on x, with above room temperature T_C observed in some compounds (e.g., $T_C = 310$ K for Cr_2Te_3 ($x = 1/3$), and 340 K for Cr_3Te_4 ($x = 0.5$)) [35,38]. Considering that T_C and magnetic anisotropy are key factors that determine various magnetic and spin-transport properties, the tunability of these material parameters suggest that $Cr_{1+x}Te_2$ is an adequate material which can be readily customized for desired device characteristics.

In this work, we apply a post-growth ex-situ process to effectively modulate the magnetic properties of Cr_2Te_3 ultra-thin films. This is distinct from earlier studies, in which the magnetic properties of $Cr_{1+x}Te_2$ were pre-determined during the growth process via stoichiometry or thickness control [32,35,39]. Here, we observe that the T_C and magnetic anisotropy of the Cr_2Te_3 films are significantly changed by post-growth annealing. As-grown Cr_2Te_3 (8 nm) show $T_C \sim 170$ K and out-of-plane (OOP) magnetic easy axis; high temperature (300–400 °C) ex-situ annealing results in the enhancement of its T_C up to room temperature (~ 300 K) and the reorientation of its magnetic easy axis to the in-plane (IP) direction. We observe a noticeable expansion (> 3 %) of the c-axis lattice constant upon post-growth annealing, whereas electronic, chemical, and structural analysis show that neither the chemical stoichiometry nor overall atomic structure is hardly affected by the annealing process. Therefore, we presume the annealing-induced c-axis expansion to be the origin of the modulation of the Cr_2Te_3 film magnetic properties. Our findings illustrate a practical ex-situ process to not only control the magnetic properties, but also achieve room temperature ferromagnetism in Cr_2Te_3 thin films. The robust ferromagnetic ordering even after high temperature annealing (up to 400 °C) in atmospheric conditions suggest that the Cr_2Te_3 films are vdW magnetic materials that are suitable for potential technological applications in spintronic devices. Furthermore, we propose that this annealing-induced lattice constant modulation method could potentially be applied to finely tune material characteristics of other quantum materials, given that the lattice constant is a key factor that determines electronic, spin, charge, and orbital properties of various transition metal chalcogenide (TMC) material systems [20,40,41].

2. Experimental section

8-nm-thick Cr_2Te_3 thin films are grown on sapphire substrates (0001) in a high-vacuum co-evaporation chamber with base pressure lower than 5×10^{-8} Torr. In order to prevent oxidation, 2-nm-thick Al capping layers are deposited on the top. Details of the Cr_2Te_3 thin film growth process is explained in a previous report [34]. Following the growth, an annealing process is performed in atmospheric conditions for 30 min at various temperatures in the range of 100–400 °C.

The magnetic hysteresis loops of the films are measured by vibrating sample magnetometry (VSM). The measurements are carried out in in-plane (magnetic field parallel to the film plane; IP) and out-of-plane (magnetic field perpendicular to the film plane; OOP) geometries, and as a function of temperature (110–300 K). Temperature-dependent resistance and magnetoresistance measurements are performed using a commercial Hall effect measurement system (Seongwoo Instruments Inc.). Magnetic fields up to 1.3 T are applied, and the measuring temperature range is 10–340 K. Measurements are carried out in the van der Pauw geometry with square-shaped thin film samples.

X-ray absorption spectroscopy (XAS) and x-ray magnetic circular dichroism (XMCD) are carried out at the 2A and 6A beamlines at the Pohang Light Source (PLS-II). The total electron yield mode, with an energy resolution of ~ 0.1 eV, is used for the measurements. The sample current is divided by the photon beam current to remove any effects of variation in beam intensity. The base pressure of the analysis chamber is 9×10^{-10} Torr. For XMCD measurements, external magnetic fields of $H = \pm 0.65$ T are applied with circularly polarized x-rays. The magnetic field direction is set to 0° and 80° with respect to the surface normal direction for the OOP and IP measurement geometries, respectively. The angle of the incident x-ray is tilted 22.5° from the surface normal direction.

Structural properties of the samples are characterized by cross-sectional high-resolution transmission electron microscopy (TEM) and x-ray diffraction (XRD). The TEM specimens are prepared by a focused ion beam (Hitachi; NX5000) using Ga and Ar ions. Bright-field TEM (BFTEM) and high-resolution high-angle annular dark field scanning TEM (HAADF-STEM) images are acquired using monochromated and Cs-corrected TEM (FEI;Titan S80 − 300) equipped with a Gatan energy filter (GATAN; GIF Quantum ERS System, model 966). For qualitative analysis and determination of the a- and c-axis lattice parameters, normal incidence high-resolution XRD (HRXRD; Empyrean, PANalytical) is measured.

3. Results and discussion

3.1. Magnetic properties of as-grown and ex-situ annealed Cr_2Te_3 thin films

The effect of the ex-situ annealing process on the magnetic properties of 8-nm-thick Cr_2Te_3 thin films are investigated by measuring its magnetic hysteresis loops (magnetic-field (H)-dependent magnetization (M) curves, i.e., M–H curves). The annealing-temperature (T_A)-dependent OOP (H // c) and IP ($H \perp c$) M–H curves of the Cr_2Te_3 films, measured by VSM, are shown in Fig. 1(a)-(h). For the as-grown and $T_A = 100$ °C annealed Cr_2Te_3 films, the OOP M–H curves show square-like loops (Fig. 1(a) and (c)), while the IP M–H curves (Fig. 1(b) and (d)) show negligible magnetic signals up to 2 T, which indicate that the as-grown and $T_A = 100$ °C Cr_2Te_3 films possess perpendicular magnetic anisotropy (PMA) similar to the molecular beam epitaxy (MBE)-grown films reported in previous studies [32,34,39,42,43]. We also see that the OOP magnetic signal disappears at 200 K (green lines in Fig. 1(a) and (c)), implying that T_C is below 200 K for the as-grown and $T_A = 100$ °C Cr_2Te_3 films. Unlike the as-grown and $T_A = 100$ °C films, Cr_2Te_3 films grown at $T_A = 200$ °C show saturation behavior with less than 0.5 T applied field along both the OOP (Fig. 1(e)) and IP (Fig. 1(f)) directions. Furthermore, the $T_A = 200$ °C films show magnetic signals at 200 K for both OOP and IP magnetic fields (green lines in Fig. 1(e) and (f)), and in particular the IP magnetic signal is significantly larger than the OOP magnetic signal at 200 K. This implies that the T_C of the $T_A = 200$ °C film exceeds 200 K, and also suggests the presence of mixed magnetic phases with distinct magnetic anisotropies and transition temperatures. For the $T_A = 200$ °C annealing condition, it is possible that one magnetic phase prefers OOP magnetization with lower transition temperature (~ 170 K) similar to the bulk Cr_2Te_3 magnetic phase, while the other phase prefers IP magnetization with higher transition temperature (~ 250 K) similar to the high T_C phases of Cr_2Te_3 films previously reported [34]. Annealing at higher temperatures gives rise to more significant change. For the $T_A = 400$ °C Cr_2Te_3 films, the OOP M–H curves (Fig. 1(g)) show small magnetic signals with no remanent magnetization, while the IP M–H curves (Fig. 1(h)) show square-like hysteresis loops up to 300 K. Thus, the 400 °C annealing process has changed the Cr_2Te_3 film magnetic easy axis from OOP to IP and simultaneously enhanced the T_C of the film to room temperature.

The annealing-induced magnetic properties modulation of the

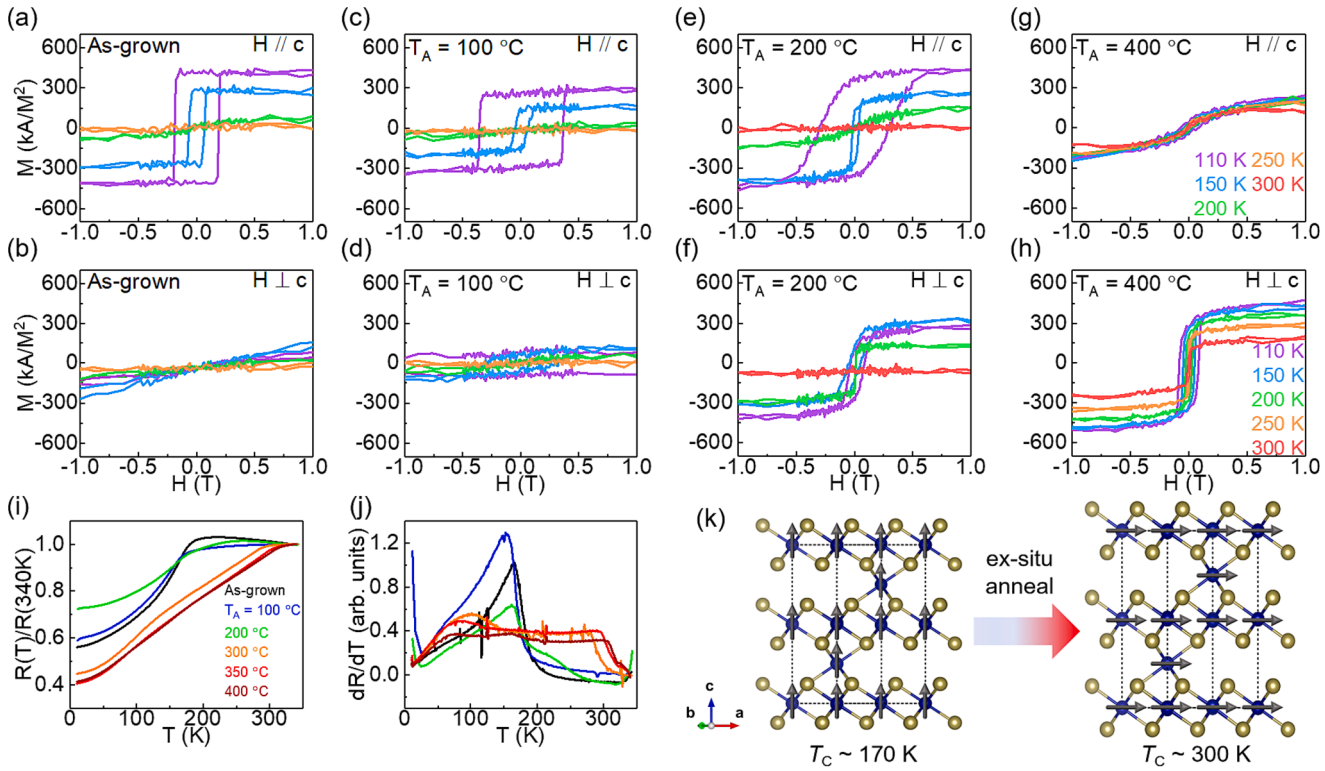

Fig. 1. Annealing-induced change of the magnetic and transport characteristics of Cr_2Te_3 thin films. (a)-(h) Magnetic-field (H)-dependent magnetization (M) of as-grown and ex-situ annealed Cr_2Te_3 films, measured at different temperatures, using VSM. Measurement data for (a)-(b) as-grown films, (c)-(d) $T_A = 100$ °C films, (e)-(f) $T_A = 200$ °C films, and (g)-(h) $T_A = 400$ °C films. (a), (c), (e), and (g) show the OOP M–H curves, and (b), (d), (f), and (h) show the IP M–H curves. (i) Residual resistance ratio of the as-grown and ex-situ annealed Cr_2Te_3 films. Residual resistance ratio was derived by dividing the temperature-dependent resistance $R(T)$ by the resistance at 340 K. (j) Derivative of the $R(T)$ data, i.e., dR/dT. (k) Schematics of the annealing-induced magnetic properties modulation.

Cr_2Te_3 film is further investigated by temperature-dependent resistance (R-T) measurements. Typically, in ferromagnetic metal systems, R-T curves show changes in its slope at a magnetic transition temperature owing to changes in the magnetic-ordering-induced spin scattering [31]. The temperature-dependent residual resistance ratio (resistance at a certain temperature divided by the resistance at 340 K) and its derivative are shown in Fig. 1(i) and (j), respectively. The as-grown and $T_A = 100$ °C films show a single slope change around 170 K (black and blue curves in Fig. 1(i) and (j)) indicating that $T_C \sim 170$ K for the as-grown and $T_A = 100$ °C films. The $T_A = 200$ °C Cr_2Te_3 films show slope change at two different temperatures, one near 170 K and another near 250 K; this is clearly seen in the R-T curve inflections points determined from the derivative of the residual resistance ratio (see green curve in Fig. 1(j)). This suggests that the $T_A = 200$ °C films might have mixed magnetic phases with two distinct magnetic transition temperatures, as discussed earlier. The Cr_2Te_3 films annealed at higher T_A (≥ 300 °C) show inflection points near room temperature (see Fig. 1(j)), confirming that the T_C of the Cr_2Te_3 films is enhanced by the ex-situ annealing process. Overall, the residual resistance ratio curves clearly demonstrate the presence of two distinct magnetic phases: (1) the as-grown and $T_A = 100$ °C films, and (2) the $T_A = 300$–400 °C films, with the $T_A = 200$ °C films in the transition process. The T_A-dependent M–H and R-T measurement results show that the ex-situ annealing process can be effectively utilized to control both the T_C and magnetic anisotropy of the Cr_2Te_3 films, as schematically shown in Fig. 1(k). In the following, we will find that the origin of annealing effect is the c-lattice expansion as depicted in Fig. 1(k). The threshold T_A for this magnetic property modulation effect to occur is estimated to be 200 °C, with the possibility of mixed magnetic phases for the $T_A = 200$ °C films. In Supplementary Material (SM) Fig. S1 and discussion, we show temperature-dependent magnetoresistance data which further validate the annealing effect on the Cr_2Te_3 magnetic properties.

3.2. XAS and XMCD analyses of as-grown and ex-situ annealed Cr_2Te_3 thin films

In order to explore the origin of the annealing-induced magnetic property modulation, electronic, magnetic, and structural analyses are carried out. First, the local electronic character and the magnetic ground state of the Cr_2Te_3 films are examined using XAS and XMCD spectroscopy measured at the Cr $L_{2,3}$ x-ray absorption edges. Temperature-dependent XAS (upper panels in Fig. 2) are measured in two different geometries: OOP geometry in which the x-ray beam has near normal incidence (incident angle = 22.5°), and IP geometry in which the beam is incident at a smaller angle (incident angle = 57.5°). XMCD (lower panels in Fig. 2) is defined as the asymmetry ratio between the XAS measured with a 0.65 T magnetic field applied anti-parallel (μ^-) and parallel (μ^+) to the x-ray helicity. The XAS spectra of the Cr_2Te_3 films (upper panels in Fig. 2) show two different peaks at approximately 575 eV and 584 eV, corresponding to the Cr L_3 edges and L_2 edges, respectively. The XAS spectra are in good agreement with previous reports on Cr_2Te_3 films [34,44,45], which suggest that the Cr_2Te_3 phase is well formed in our films. We note that the Te $M_{4,5}$ x-ray absorption edges, which are also present in the measured x-ray energy range, shows negligible contribution to the XAS spectra due to the low integrated XAS intensity compared to the Cr $L_{2,3}$-edges [44,45].

We observe that all the Cr_2Te_3 films show nearly identical XAS spectra, regardless of T_A, with the exception of a small shoulder peak appearing for the $T_A = 400$ °C films. This implies that the post-growth ex-situ annealing process has minimal effect on the chemical stoichiometry of the Cr_2Te_3 films. The small shoulder peaks near 577 eV in Fig. 2(g) and (h) are located at the x-ray absorption energy of the oxidized Chromium [45]. Hence, we presume that the top surface of the Cr_2Te_3 films is partially oxidized, possibly due to the high annealing temperature ($T_A = 400$ °C) in atmospheric conditions. However, the

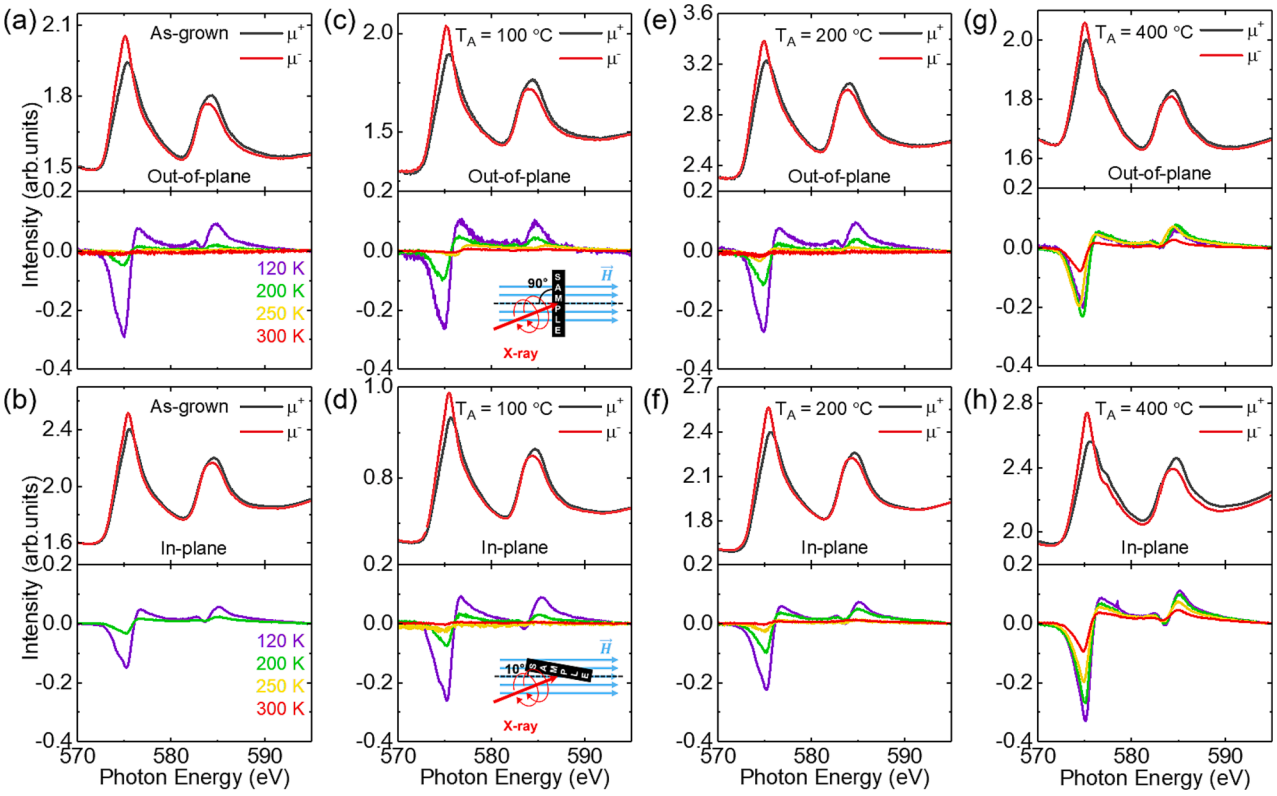

Fig. 2. XAS and XMCD data of the as-grown and ex-situ annealed Cr_2Te_3 films. Measurements are done in OOP ((a), (c), (e), (g)) and IP ((b), (d), (f), (h)) geometries; measurement schematics shown as insets in (c) and (d). Upper panels of each graph show the XAS spectra with the magnetic field applied parallel (μ^+, black line) and anti-parallel (μ^-, red line) to the x-ray helicity, measured at 120 K. Lower panels show the XMCD spectra (difference in the μ^+ and μ^- XAS spectra divided by the sum). (For interpretation of the references to colour in this figure legend, the reader is referred to the web version of this article.)

intensity of the shoulder peak is much smaller than the main Cr L_3 edge peak, and in the following XMCD analysis, we show that the shoulder peak shows no contribution to the magnetic signal of the Cr_2Te_3 films. Furthermore, we will also show that there are no detectible levels of Cr_2O_3 XRD peaks observed for annealing temperature up to 350 °C (see section 3.4). These observations suggest that the partial oxidization of the film surface has negligible effect on its physical or magnetic properties. Overall, the shapes and features of the XAS spectra show minimal T_A-dependent change. Additionally, the chemical stoichiometry determined from Rutherford back scattering (RBS) spectroscopy also do not show any significant annealing effect (SM Fig. S2). Therefore, we conclude that the ex-situ annealing process does not affect the chemical stoichiometry or electronic structure of the Cr_2Te_3 films.

The magnetic properties of the ex-situ annealed Cr_2Te_3 films are further investigated by XMCD. XMCD spectroscopy is extensively utilized to quantify element-specific magnetic moments [46,47]. The XMCD spectra are measured in the OOP (lower panels in Fig. 2(a), (c), (e), and (g); see measurement scheme in Fig. 2(c) inset) and IP (lower panels in Fig. 2(b), (d), (f), and (h); see scheme in Fig. 2(d) inset) geometries in order to find the magnetic easy axis. The XMCD spectra of all the Cr_2Te_3 films show maximum values at the Cr L_3 edge peak position, which indicates that the magnetic signal of the Cr_2Te_3 films originate from the 3*d*-electron states in the Cr [47]. The OOP and IP XMCD intensities of the as-grown and T_A = 100 °C films (Fig. 2(a)-(d)) show significant decrease at 200 K, and the XMCD vanishes at 250 K. On the other hand, the T_A = 400 °C Cr_2Te_3 film shows OOP and IP XMCD signals up to 250 K and 300 K, suggesting that the T_C of the Cr_2Te_3 film has increased by ex-situ annealing at 400 °C. We also observe that the OOP XMCD signal is larger than the IP XMCD signal for the as-grown and T_A = 100 °C films, whereas the IP signal is larger for the T_A = 400 °C films. This suggests that the magnetic easy axis changes from OOP to IP upon high temperature ex-situ annealing, in agreement with the *M*–*H* loop results shown in Fig. 1. Note that the XMCD of the as-grown and T_A = 100 °C films in the IP geometry, and the XMCD of the T_A = 400 °C films in the OOP geometry show sizeable magnetic signals despite the change in magnetic easy axis; this is possibly due to the large (0.65 T) magnetic field not being applied completely IP or OOP (see schematics in the insets of Fig. 2(c) and (d)) such that the Cr_2Te_3 film magnetization is slightly canted in both measurement geometries. Nevertheless, the XMCD measurements confirm that the magnetic properties of the Cr_2Te_3 films can be effectively modulated by ex-situ annealing.

3.3. TEM measurement of as-grown and ex-situ annealed Cr_2Te_3 thin films

Given the absence of any ex-situ annealing effect on the chemical or electronic properties, we examine possible annealing-induced changes in the atomic structure of the Cr_2Te_3 films by performing cross-sectional TEM measurements (Fig. 3). The BFTEM images (Fig. 3(a) and (c)) and HAADF-STEM images (Fig. 3(b) and (d)) show the atomic structure of the Cr_2Te_3 films processed with two different ex-situ annealing conditions (T_A = 200 °C and T_A = 400 °C). The TEM images show the epitaxial quality of the annealed Cr_2Te_3 films, with the atomic structure remaining intact even after ex-situ annealing. The fast Fourier transform (FFT) image obtained from the Cr_2Te_3 films (insets in Fig. 3(a) and (c)) shows alignment along the [1120] direction, i.e, the in-plane structure of the Cr_2Te_3 films are oriented with that of the sapphire substrates. In between the Cr_2Te_3 films and the substrate, a few-nm thick amorphous layer is observed. We presume this to be a complex mixture of Al-O-Te, which have been also observed in previous studies on Cr_2Te_3 films [34,39]; the formation of the amorphous layer at the film-substrate interface is possibly due to the high Te flux ratio during formations of the seed layer. The TEM measurements show that the annealed Cr_2Te_3 films have nearly identical atomic structures with the as-grown Cr_2Te_3

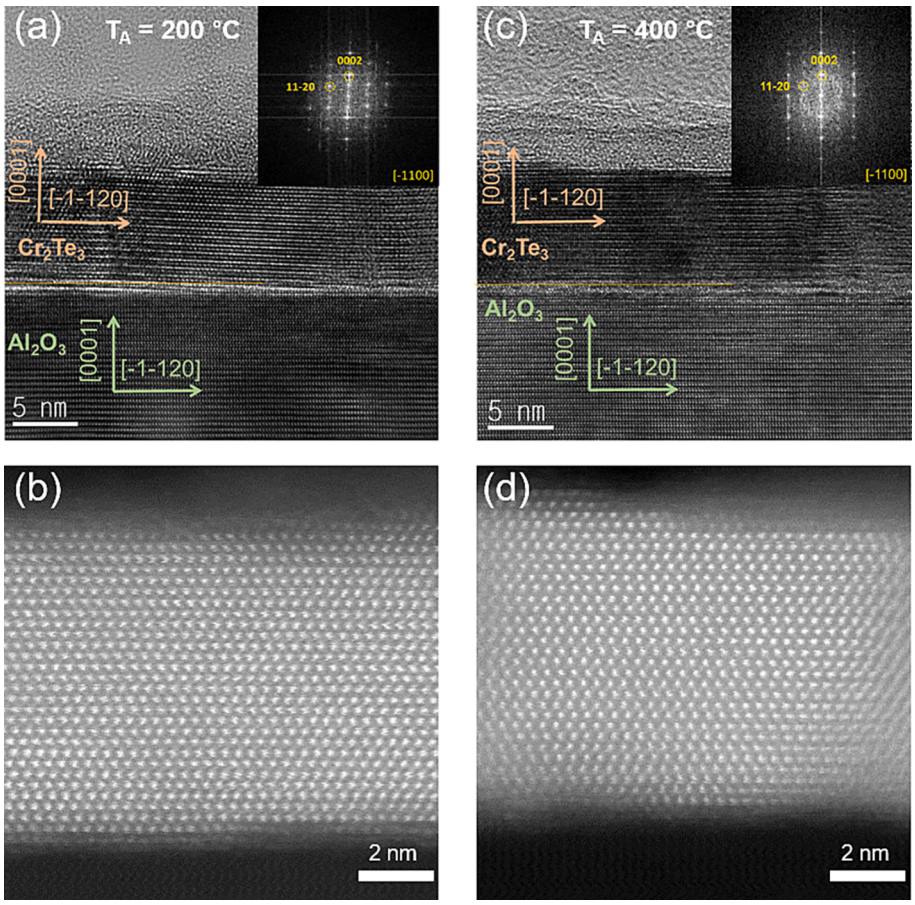

Fig. 3. Cross-sectional TEM images of Cr_2Te_3 films with two different ex-situ annealing conditions. TEM images shown for (a, b) T_A = 200 °C films, and (c, d) T_A = 400 °C films. BFTEM and respective FFT pattern images (inset) are shown in (a, c), and HAADF-STEM images are shown in (b, d).

films reported earlier [34], suggesting that the qualitative structural properties of the films are not affected by ex-situ annealing. The TEM images of the annealed Cr_2Te_3 films also do not show measurable levels of diffused oxygen or Al impurities. Another noticeable annealing-dependent change is that the thickness of the interfacial amorphous layer tends to decrease when the annealing temperature is increased, which might be related to an ex-situ-annealing-induced recrystallization process [48].

3.4. *Ex-situ-annealing-induced change of the Cr_2Te_3 lattice parameters measured by XRD*

While the overall atomic structure of the films is not affected by the annealing process, we further examine any possible annealing-induced changes in the lattice constant of the Cr_2Te_3 films by measuring high-resolution XRD. The θ-2θ scans (Fig. 4(a) and (b)) show two diffraction peaks near 30° and 60°, which correspond to Cr_2Te_3 (0 0 4) and Cr_2Te_3 (0 0 8), respectively, suggesting that the Cr_2Te_3 films are well grown. Both (0 0 4) and (0 0 8) diffraction peaks shift to lower angles when T_A increases (Fig. 4(a) and (b)), indicating that the ex-situ

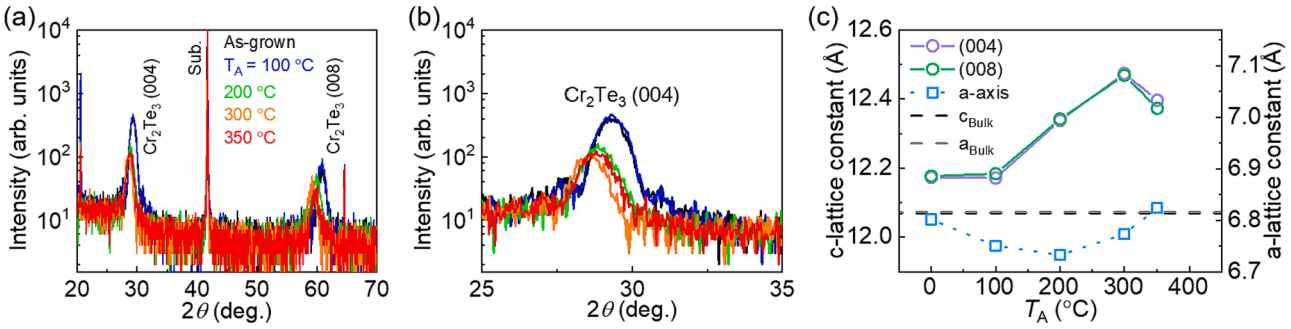

Fig. 4. Annealing-induced change of the Cr_2Te_3 thin film lattice constants. (a, b) XRD θ-2θ data of the as-grown and ex-situ annealed Cr_2Te_3 films. (a) Wide range (20–70 degree) XRD data showing two different Cr_2Te_3 diffraction peaks (0 0 4) and (0 0 8), along with the substrate (sapphire) diffraction peak. (b) Zoomed-in view of the Cr_2Te_3 (0 0 4) diffraction peaks. (c) T_A-dependent lattice constants of the Cr_2Te_3 films derived from the diffraction peak positions. The c-axis lattice constants are determined from the (0 0 4) and (0 0 8) peaks in (a) and (b), whereas the a-axis lattice constants are calculated from the (1 1 2) diffraction peaks shown in SM Fig. S3. Bulk c-axis and a-axis lattice constants are indicated by the black and grey dashed lines.

annealing process affects the Cr_2Te_3 lattice parameter. The c-axis lattice constants of the Cr_2Te_3 films are calculated from the (0 0 4) and (0 0 8) diffraction peak positions using Bragg's law, and are plotted as a function of T_A in Fig. 4(c) (circular data points). The c-axis lattice constant of the as-grown and T_A = 100 °C Cr_2Te_3 films shows similar values (~ 12.17 Å) with that of previous reported Cr_2Te_3 films grown on sapphire substrates [34]. We observe that the c-axis lattice constants of films significantly increase for $T_A \geq 200$ °C. The $T_A = 200$ °C films show c-axis lattice constant of 12.34 Å (2.2 % increase compared to the Cr_2Te_3 bulk), and the $T_A = 300$ °C films show the maximum c-axis lattice constant of 12.47 Å (3.3 % increase compared to the Cr_2Te_3 bulk). Note that T_A = 200 °C was the annealing temperature at which the Cr_2Te_3 films started to exhibit two peaks in the dR/dT curve (Fig. 2(j)). We also evaluate the T_A-dependent a-axis lattice constant of the Cr_2Te_3 films derived from the (1 1 2) diffraction peaks (See SM Fig. S3). In contrast to the large T_A-dependent change in the c-axis lattice constant, the a-axis lattice constant (square data points in Fig. 4(c)) shows relatively small changes (~ -1 %) compared to the c-axis lattice constant. In the following section, we will see that this T_A-dependent increase of the c-axis lattice constant is the most likely origin of the annealing-induced change in the Cr_2Te_3 thin film magnetic properties.

3.5. Possible origins of ex-situ-annealing-induced modulation of the Cr_2Te_3 film properties

We discuss possible causes for the c-axis lattice expansion and the magnetic properties modulation of the Cr_2Te_3 thin films, which are both seemingly induced by high temperature annealing. For this, we first show experimental data which demonstrates that the ex-situ process is a key requirement for the magnetic property modulation observed in this work. In SM Fig. S4, the magnetic properties of the as-grown and *in-vacuum*-annealed Cr_2Te_3 thin films are compared. We see that T_C of the in-vacuum-annealed Cr_2Te_3 thin film slightly increases by ~ 30 K, yet the overall magnetic properties of the Cr_2Te_3 thin film annealed in vacuum shows minimal change with respect to the as-grown film (SM Fig. S4), in contrast to the dramatic modulation observed for the ex-situ annealed Cr_2Te_3 thin films.

Possible annealing-induced changes in the Cr-Te composition is also discussed. In section 3.2, we stated that RBS measurements show little annealing-induced change in the thin film composition (see SM Fig. S2). Despite some inaccuracies (±5 atomic %) in the RBS analysis, the Cr-Te composition is still far away from the other $Cr_{1+x}Te_2$ phases [35–38,49]. This is in contrast to Ref. 49, in which annealing-induced compositional change, particularly the emergence of a high-T_C Cr_3Te_4 phase, was observed upon in-vacuum annealing of Cr_2Te_3 thin films. Additionally, it should be noted that the TEM images of the annealed films (Fig. 3) highly resemble those of as-grown Cr_2Te_3 thin films [34]. The absence of any significant in-vacuum annealing effect or any significant compositional change suggest that the origin of the annealing-induced magnetic property modulation observed in our work is distinct from the compositional change mechanism suggested in Ref. 49. Here, given the presence of Al capping layers on top of all the Cr_2Te_3 films investigated, it is quite possible that ex-situ-annealing-induced oxidation of the Al layer might be the origin of the annealing effect. A volume change in the Al layer, associated with the oxidation process, may cause a strain effect on the adjacent Cr_2Te_3 film leading to changes in the c-axis and a-axis lattice constants seen in Fig. 4(c). For full validation of the proposed Al-oxidation-induced strain effect mechanism, a thorough investigation comparing the structural, chemical, and magnetic properties of Cr_2Te_3 films annealed under various conditions is required in follow-up studies.

In order to understand the c-lattice-expansion-dependent change in the Cr_2Te_3 magnetic properties, we refer to earlier studies which show that the c-axis lattice expansion can result in significant enhancement of T_C, along with change in the magnetic easy axis [34,35]. In those reports, experimental measurements were corroborated by theoretical calculations which confirm that the magnetic properties of Cr_2Te_3 thin films are highly sensitive to the c-lattice parameter. We believe a similar explanation is applicable to our current results. However, in contrast to earlier studies in which the extended c-axis was incorporated during the film growth phase (via elemental flux control or film thickness control), we use a post-growth ex-situ annealing process to activate the c-axis expansion and subsequent large modulation in the magnetic properties of the Cr_2Te_3 films. We propose that this simple post-growth annealing process could be applied to control emergent quantum phenomena in other telluride and selenide compounds. For instance, spin, charge, orbital, and band topologies of many TMC materials (e.g., VSe_{2-x} [40], $NiTe_{2-x}Se_x$ [20], $PtTe_x$ [41]) are highly dependent on the lattice, such that our lattice parameter modulation method may potentially be used to finely tune key material properties.

4. Conclusion

In this experimental study, we show that the magnetic properties of 8-nm-thick Cr_2Te_3 thin films can be controlled via ex-situ annealing. High-temperature (300–400 °C) annealing leads to significant enhancement of T_C (increase from 170 to 300 K), along with change in the magnetic easy axis (from OOP to IP). XRD measurements show the presence of annealing-induced c-axis lattice expansion, which is the most likely origin of the modulation in the T_C and magnetic anisotropy of the Cr_2Te_3 films. Our findings demonstrate an effective and practical method to control the magnetic properties of vdW ferromagnetic thin films.

CRediT authorship contribution statement

In Hak Lee: Conceptualization, Methodology, Formal analysis, Investigation, Data curation, Writing – original draft, Writing – review & editing. **Yeong Gwang Khim:** Methodology, Formal analysis, Investigation. **Jaeun Eom:** Investigation. **Jung Yun Kee:** Investigation. **Byoung Ki Choi:** Investigation. **Hyuk Jin Kim:** Investigation. **Ryung Kim:** Investigation. **Min Young Jung:** Investigation. **Kyeong Jun Lee:** Investigation. **Younghak Kim:** Investigation, Resources. **Woo-Suk Noh:** Investigation, Resources. **Byeong-hyeon Lee:** Formal analysis, Investigation. **Hoyoung Suh:** Formal analysis, Investigation. **Hye Jung Chang:** Formal analysis, Investigation. **Sung Ok Won:** Formal analysis, Investigation. **Chaun Jang:** Investigation, Writing – review & editing. **Hyejin Ryu:** Investigation, Writing – review & editing. **Dong Ryeol Lee:** Investigation, Writing – review & editing. **Seo Hyoung Chang:** Investigation, Writing – review & editing. **Hyun Hwi Lee:** Investigation, Writing – review & editing. **Young Jun Chang:** Conceptualization, Validation, Investigation, Writing – review & editing, Supervision, Funding acquisition. **Jun Woo Choi:** Conceptualization, Methodology, Validation, Investigation, Resources, Writing – original draft, Writing – review & editing, Supervision, Project administration, Funding acquisition.

Declaration of competing interest

The authors declare that they have no known competing financial interests or personal relationships that could have appeared to influence the work reported in this paper.

Data availability

Data will be made available on request.

Acknowledgements

This work was supported by the KIST Institutional Program (2E32251, 2E32252), the National Research Foundation of Korea (NRF) grants funded by the Ministry of Science and ICT (MSIT) (NRF-2020R1A5A1016518, NRF-2021M3H4A1A03054856, NRF-

2021R1A2C2011007, NRF-2020R1A2C200373211, NRF-2021R1A6A3A14040322, RS-2023-00244143, RS-2023-00284081, RS-2023-00220471), and the Innovative Talent Education Program for Smart City by MOLIT.

Appendix A. Supplementary material

Supplementary data to this article can be found online at https://doi.org/10.1016/j.apsusc.2023.159057.

References

[1] C. Gong, L. Li, Z. Li, H. Ji, A. Stern, Y. Xia, T. Cao, W. Bao, C. Wang, Y. Wang, Z. Q. Qiu, R.J. Cava, S.G. Louie, J. Xia, X. Zhang, Discovery of intrinsic ferromagnetism in two-dimensional van der Waals crystals, Nature 546 (2017) 265–269.

[2] B. Huang, G. Clark, E. Navarro-Moratalla, D.R. Klein, R. Cheng, K.L. Seyler, D. Zhong, E. Schmidgall, M.A. McGuire, D.H. Cobden, W. Yao, D. Xiao, P. Jarillo-Herrero, X. Xu, Layer-dependent ferromagnetism in a van der Waals crystal down to the monolayer limit, Nature 546 (2017) 270–273.

[3] Z. Fei, B. Huang, P. Malinowski, W. Wang, T. Song, J. Sanchez, W. Yao, D. Xiao, X. Zhu, A.F. May, W. Wu, D.H. Cobden, J.-H. Chu, X. Xu, Two-dimensional itinerant ferromagnetism in atomically thin Fe_3GeTe_2, Nat. Mater. 17 (2018) 778–782.

[4] B. Huang, G. Clark, D.R. Klein, D. MacNeill, E. Navarro-Moratalla, K.L. Seyler, N. Wilson, M.A. McGuire, D.H. Cobden, D. Xiao, W. Yao, P. Jarillo-Herrero, X. Xu, Electrical control of 2D magnetism in bilayer CrI_3, Nat. Nanotechnol. 13 (2018) 544–548.

[5] K.-H. Min, D.H. Lee, S.-J. Choi, I.-H. Lee, J. Seo, D.W. Kim, K.-T. Ko, K. Watanabe, T. Taniguchi, D.H. Ha, C. Kim, J.H. Shim, J. Eom, J.S. Kim, S. Jung, Tunable spin injection and detection across a van der Waals interface, Nat. Mater. 21 (2022) 1144–1149.

[6] Y. Chen, Y. Zhu, R. Lin, W. Niu, R. Liu, W. Zhuang, X. Zhang, J. Liang, W. Sun, Z. Chen, Y. Hu, F. Song, J. Zhou, D. Wu, B. Ge, H. Yang, R. Zhang, X. Wang, Observation of Colossal Topological Hall Effect in Noncoplanar Ferromagnet Cr_5Te_6 Thin Films, Adv. Funct. Mater. 33 (2023) 2302984.

[7] S.Y. Lim, K. Kim, S. Lee, J.-G. Park, H. Cheong, Thickness dependence of antiferromagnetic phase transition in Heisenberg-type $MnPS_3$, Curr. Appl Phys. 21 (2021) 1–5.

[8] D.S. Kim, J.Y. Kee, J.-E. Lee, Y. Liu, Y. Kim, N. Kim, C. Hwang, W. Kim, C. Petrovic, D.R. Lee, C. Jang, H. Ryu, J.W. Choi, Surface oxidation in a van der Waals ferromagnet $Fe_{3-x}GeTe_2$, Curr. Appl Phys. 30 (2021) 40–45.

[9] S.W. Cho, I.H. Lee, Y. Lee, S. Kim, Y.G. Khim, S.-Y. Park, Y. Jo, J. Choi, S. Han, Y. J. Chang, S. Lee, Investigation of the mechanism of the anomalous Hall effects in Cr2Te3/(BiSb)2(TeSe)3 heterostructure, Nano Convergence 10 (2023) 2.

[10] J. Ji, H.-M. Kwak, J. Yu, S. Park, J.-H. Park, H. Kim, S. Kim, S. Kim, D.-S. Lee, H. S. Kum, Understanding the 2D-material and substrate interaction during epitaxial growth towards successful remote epitaxy: a review, Nano Convergence 10 (2023) 19.

[11] J. Eom, I.H. Lee, J.Y. Kee, M. Cho, J. Seo, H. Suh, H.-J. Choi, Y. Sim, S. Chen, H. J. Chang, S.-H. Baek, C. Petrovic, H. Ryu, C. Jang, Y.D. Kim, C.-H. Yang, M.-J. Seong, J.H. Lee, S.Y. Park, J.W. Choi, Voltage control of magnetism in $Fe_{3-x}GeTe_2/In_2Se_3$ van der Waals ferromagnetic/ferroelectric heterostructures, Nat. Commun. 14 (2023) 5605.

[12] H.K. Gweon, S.Y. Lee, H.Y. Kwon, J. Jeong, H.J. Chang, K.-W. Kim, Z.Q. Qiu, H. Ryu, C. Jang, J.W. Choi, Exchange Bias in Weakly Interlayer-Coupled van der Waals Magnet Fe_3GeTe_2, Nano Lett. 21 (2021) 1672–1678.

[13] S.Y. Park, D.S. Kim, Y. Liu, J. Hwang, Y. Kim, W. Kim, J.-Y. Kim, C. Petrovic, C. Hwang, S.-K. Mo, H.-J. Kim, B.-C. Min, H.C. Koo, J. Chang, C. Jang, J.W. Choi, H. Ryu, Controlling the Magnetic Anisotropy of the van der Waals Ferromagnet Fe_3GeTe_2 through Hole Doping, Nano Lett. 20 (2020) 95–100.

[14] C. Gong, X. Zhang, Two-dimensional magnetic crystals and emergent heterostructure devices, Science 363 (2019) eaav4450.

[15] B. Huang, M.A. McGuire, A.F. May, D. Xiao, P. Jarillo-Herrero, X. Xu, Emergent phenomena and proximity effects in two-dimensional magnets and heterostructures, Nat. Mater. 19 (2020) 1276–1289.

[16] Y. Wu, S. Zhang, J. Zhang, W. Wang, Y.L. Zhu, J. Hu, G. Yin, K. Wong, C. Fang, C. Wan, X. Han, Q. Shao, T. Taniguchi, K. Watanabe, J. Zang, Z. Mao, X. Zhang, K. L. Wang, Néel-type skyrmion in WTe_2/Fe_3GeTe_2 van der Waals heterostructure, Nat. Commun. 11 (2020) 3860.

[17] M. Yang, Q. Li, R.V. Chopdekar, R. Dhall, J. Turner, J.D. Carlström, C. Ophus, C. Klewe, P. Shafer, A.T. N'Diaye, J.W. Choi, G. Chen, Y.Z. Wu, C. Hwang, F. Wang, Z.Q. Qiu, Creation of skyrmions in van der Waals ferromagnet Fe3GeTe2 on (Co/Pd)n superlattice, Science, Advances 6 (2020) eabb5157.

[18] M. Gibertini, M. Koperski, A.F. Morpurgo, K.S. Novoselov, Magnetic 2D materials and heterostructures, Nat. Nanotechnol. 14 (2019) 408–419.

[19] C. Zhang, C. Liu, J. Zhang, Y. Yuan, Y. Wen, Y. Li, D. Zheng, Q. Zhang, Z. Hou, G. Yin, K. Liu, Y. Peng, X.-X. Zhang, Room-Temperature Magnetic Skyrmions and Large Topological Hall Effect in Chromium Telluride Engineered by Self-Intercalation, Adv. Mater. 35 (2023) 2205967.

[20] N.H. Lam, P.L. Nguyen, B.K. Choi, T.T. Ly, G. Duvjir, T.G. Rhee, Y.J. Jo, T.H. Kim, C. Jozwiak, A. Bostwick, E. Rotenberg, Y. Hwang, Y.J. Chang, J. Lee, J. Kim, Controlling Spin-Orbit Coupling to Tailor Type-II Dirac Bands, ACS Nano 16 (2022) 11227–11233.

[21] J. Son, B. Marfoua, J. Hong, Strain dependent magnetic properties of 1T-VSe_2 monolayer, J. Korean Phys. Soc. 81 (2022) 133–138.

[22] H.J. Kim, B.K. Choi, I.H. Lee, M.J. Kim, S.-H. Chun, C. Jozwiak, A. Bostwick, E. Rotenberg, Y.J. Chang, Electronic structure and charge-density wave transition in monolayer VS_2, Curr. Appl Phys. 30 (2021) 8–13.

[23] R. Kim, B.K. Choi, K.J. Lee, H.J. Kim, H.H. Lee, T.G. Rhee, Y.G. Khim, Y.J. Chang, S. H. Chang, Atomic arrangement of van der Waals heterostructures using X-ray scattering and crystal truncation rod analysis, Curr. Appl Phys. 46 (2023) 70–75.

[24] D.L. Cortie, G.L. Causer, K.C. Rule, H. Fritzsche, W. Kreuzpaintner, F. Klose, Two-Dimensional Magnets: Forgotten History and Recent Progress towards Spintronic Applications, Adv. Funct. Mater. 30 (2020) 1901414.

[25] Q.H. Wang, A. Bedoya-Pinto, M. Blei, A.H. Dismukes, A. Hamo, S. Jenkins, M. Koperski, Y. Liu, Q.-C. Sun, E.J. Telford, H.H. Kim, M. Augustin, U. Vool, J.-X. Yin, L.H. Li, A. Falin, C.R. Dean, F. Casanova, R.F.L. Evans, M. Chshiev, A. Mishchenko, C. Petrovic, R. He, L. Zhao, A.W. Tsen, B.D. Gerardot, M. Brotons-Gisbert, Z. Guguchia, X. Roy, S. Tongay, Z. Wang, M.Z. Hasan, J. Wrachtrup, A. Yacoby, A. Fert, S. Parkin, K.S. Novoselov, P. Dai, L. Balicas, E.J.G. Santos, The Magnetic Genome of Two-Dimensional van der Waals Materials, ACS Nano 16 (2022) 6960–7079.

[26] H. Yang, S.O. Valenzuela, M. Chshiev, S. Couet, B. Dieny, B. Dlubak, A. Fert, K. Garello, M. Jamet, D.-E. Jeong, K. Lee, T. Lee, M.-B. Martin, G.S. Kar, P. Sénéor, H.-J. Shin, S. Roche, Two-dimensional materials prospects for non-volatile spintronic memories, Nature 606 (2022) 663–673.

[27] Q.X. Guo, K. Wang, H. Bai, Z.C. Zheng, L.H. Wang, X.M. Wang, W. He, G.H. Yu, J. Teng, T. Zhu, Ultra-high thermal stability of perpendicular magnetic anisotropy in the W buffered CoFeB/MgO stacks with Zr dusting layers, Appl. Phys. Lett. 120 (2022).

[28] L. Thomas, G. Jan, J. Zhu, H. Liu, Y.-J. Lee, S. Le, R.-Y. Tong, K. Pi, Y.-J. Wang, D. Shen, R. He, J. Haq, J. Teng, V. Lam, K. Huang, T. Zhong, T. Torng, P.-K. Wang, Perpendicular spin transfer torque magnetic random access memories with high spin torque efficiency and thermal stability for embedded applications (invited), J. Appl. Phys. 115 (2014).

[29] K. Lee, I.H. Lee, Y.G. Khim, S.-Y. Kwon, G. Lim, J. Jung, Y.J. Chang, J.H. Lee, Nonlinear optical properties of PVD-grown Cr_2Te_3 film and its nonlinear switching application, J. Alloy. Compd. 956 (2023), 170308.

[30] H. Chi, Y. Ou, T.B. Eldred, W. Gao, S. Kwon, J. Murray, M. Dreyer, R.E. Butera, A. C. Foucher, H. Ambaye, J. Keum, A.T. Greenberg, Y. Liu, M.R. Neupane, G.J. de Coster, O.A. Vail, P.J. Taylor, P.A. Folkes, C. Rong, G. Yin, R.K. Lake, F.M. Ross, V. Lauter, D. Heiman, J.S. Moodera, Strain-tunable Berry curvature in quasi-two-dimensional chromium telluride, Nat. Commun. 14 (2023) 3222.

[31] A. Roy, S. Guchhait, R. Dey, T. Pramanik, C.-C. Hsieh, A. Rai, S.K. Banerjee, Perpendicular magnetic anisotropy and spin glass-like behavior in molecular beam epitaxy grown chromium telluride thin films, ACS Nano 9 (2015) 3772–3779.

[32] Y. Fujisawa, M. Pardo-Almanza, J. Garland, K. Yamagami, X. Zhu, X. Chen, K. Araki, T. Takeda, M. Kobayashi, Y. Takeda, C.H. Hsu, F.C. Chuang, R. Laskowski, K.H. Khoo, A. Soumyanarayanan, Y. Okada, Tailoring magnetism in self-intercalated Cr1+δTe2 epitaxial films, Physical Review Materials 4 (2020), 114001.

[33] L. Meng, Z. Zhou, M. Xu, S. Yang, K. Si, L. Liu, X. Wang, H. Jiang, B. Li, P. Qin, P. Zhang, J. Wang, Z. Liu, P. Tang, Y. Ye, W. Zhou, L. Bao, H.-J. Gao, Y. Gong, Anomalous thickness dependence of Curie temperature in air-stable two-dimensional ferromagnetic 1T-$CrTe_2$ grown by chemical vapor deposition, Nat. Commun. 12 (2021) 809.

[34] I.H. Lee, B.K. Choi, H.J. Kim, M.J. Kim, H.Y. Jeong, J.H. Lee, S.-Y. Park, Y. Jo, C. Lee, J.W. Choi, S.W. Cho, S. Lee, Y. Kim, B.H. Kim, K.J. Lee, J.E. Heo, S. H. Chang, F. Li, B.L. Chittari, J. Jung, Y.J. Chang, Modulating Curie temperature and magnetic anisotropy in nanoscale-layered Cr_2Te_3 films: implications for room-temperature spintronics, ACS Applied Nano Materials 4 (2021) 4810–4819.

[35] Y. Wen, Z. Liu, Y. Zhang, C. Xia, B. Zhai, X. Zhang, G. Zhai, C. Shen, P. He, R. Cheng, L. Yin, Y. Yao, M. Getaye Sendeku, Z. Wang, X. Ye, C. Liu, C. Jiang, C. Shan, Y. Long, J. He, Tunable room-temperature ferromagnetism in two-dimensional Cr_2Te_3, Nano Lett. 20 (2020) 3130–3139.

[36] X. Zhang, W. Liu, W. Niu, Q. Lu, W. Wang, A. Sarikhani, X. Wu, C. Zhu, J. Sun, M. Vaninger, P.F. Miceli, J. Li, D.J. Singh, Y.S. Hor, Y. Zhao, C. Liu, L. He, R. Zhang, G. Bian, D. Yu, Y. Xu, Self-Intercalation tunable interlayer exchange coupling in a synthetic van der Waals Antiferromagnet, Adv. Funct. Mater. 32 (2022) 2202977.

[37] X. Zhang, Q. Lu, W. Liu, W. Niu, J. Sun, J. Cook, M. Vaninger, P.F. Miceli, D. J. Singh, S.-W. Lian, T.-R. Chang, X. He, J. Du, L. He, R. Zhang, G. Bian, Y. Xu, Room-temperature intrinsic ferromagnetism in epitaxial $CrTe_2$ ultrathin films, Nat. Commun. 12 (2021) 2492.

[38] R. Chua, J. Zhou, X. Yu, W. Yu, J. Gou, R. Zhu, L. Zhang, M. Liu, M.B.H. Breese, W. Chen, K.P. Loh, Y.P. Feng, M. Yang, Y.L. Huang, A.T.S. Wee, Room temperature ferromagnetism of monolayer chromium telluride with perpendicular magnetic anisotropy, Adv. Mater. 33 (2021) 2103360.

[39] H. Li, L. Wang, J. Chen, T. Yu, L. Zhou, Y. Qiu, H. He, F. Ye, I.K. Sou, G. Wang, Molecular beam epitaxy grown Cr_2Te_3 thin films with tunable curie temperatures for spintronic devices, ACS Applied Nano Materials 2 (2019) 6809–6817.

[40] M. Nakano, Y. Wang, S. Yoshida, H. Matsuoka, Y. Majima, K. Ikeda, Y. Hirata, Y. Takeda, H. Wadati, Y. Kohama, Y. Ohigashi, M. Sakano, K. Ishizaka, Y. Iwasa, Intrinsic 2D Ferromagnetism in V_5Se_8 epitaxial thin films, Nano Lett. 19 (2019) 8806–8810.

[41] K. Lasek, M. Ghorbani-Asl, V. Pathirage, A.V. Krasheninnikov, M. Batzill, Controlling stoichiometry in ultrathin van der Waals Films: $PtTe_2$, Pt_2Te_3, Pt_3Te_4, and Pt_2Te_2, ACS Nano 16 (2022) 9908–9919.

[42] K. Lasek, P.M. Coelho, K. Zberecki, Y. Xin, S.K. Kolekar, J. Li, M. Batzill, Molecular beam epitaxy of transition metal (Ti-, V-, and Cr-) tellurides: from monolayer ditellurides to multilayer self-intercalation compounds, ACS Nano 14 (2020) 8473–8484.
[43] A.L. Coughlin, D. Xie, Y. Yao, X. Zhan, Q. Chen, H. Hewa-Walpitage, X. Zhang, H. Guo, H. Zhou, J. Lou, J. Wang, Y.S. Li, H.A. Fertig, S. Zhang, Near degeneracy of magnetic phases in two-dimensional chromium telluride with enhanced perpendicular magnetic anisotropy, ACS Nano 14 (2020) 15256–15266.
[44] K. Yaji, A. Kimura, C. Hirai, M. Taniguchi, M. Koyama, H. Sato, K. Shimada, A. Tanaka, T. Muro, S. Imada, S. Suga, Electronic structure of Cr1-δX (X=S, Te) studied by Cr 2p soft x-ray magnetic circular dichroism, Phys. Rev. B 70 (2004), 064402.
[45] D.M. Burn, L.B. Duffy, R. Fujita, S.L. Zhang, A.I. Figueroa, J. Herrero-Martin, G. van der Laan, T. Hesjedal, Cr_2Te_3 thin films for integration in magnetic topological insulator heterostructures, Sci. Rep. 9 (2019) 10793.
[46] C.T. Chen, Y.U. Idzerda, H.J. Lin, N.V. Smith, G. Meigs, E. Chaban, G.H. Ho, E. Pellegrin, F. Sette, Experimental confirmation of the X-ray magnetic circular dichroism sum rules for iron and cobalt, Phys. Rev. Lett. 75 (1995) 152–155.
[47] J. Stöhr, Exploring the microscopic origin of magnetic anisotropies with X-ray magnetic circular dichroism (XMCD) spectroscopy, J. Magn. Magn. Mater. 200 (1999) 470–497.
[48] E. Longo, C. Wiemer, R. Cecchini, M. Longo, A. Lamperti, A. Khanas, A. Zenkevich, M. Cantoni, C. Rinaldi, M. Fanciulli, R. Mantovan, Fe/Sb_2Te_3 interface reconstruction through mild thermal annealing, Adv. Mater. Interfaces 7 (2020) 2000905.
[49] K. Lasek, P.M. Coelho, P. Gargiani, M. Valvidares, K. Mohseni, H.L. Meyerheim, I. Kostanovskiy, K. Zberecki, M. Batzill, Van der Waals epitaxy growth of 2D ferromagnetic Cr(1+δ)Te2 nanolayers with concentration-tunable magnetic anisotropy, Appl. Phys. Rev. 9 (2022), 011409.